7-2004

Energy-Landscape-Model Analysis for Irreversibility and its Pulse-Width Dependence in Cells Subjected to a High-Intensity Ultrashort Electric Pulse

R. P. Joshi

Q. Hu

Karl H. Schoenbach
Old Dominion University

Stephen J. Beebe
Old Dominion University, sbeebe@odu.edu

Original Publication Citation

Joshi, R.P., Hu, Q., Schoenbach, K.H., & Beebe, S.J. (2004). Energy-landscape-model analysis for irreversibility and its pulse-width dependence in cells subjected to a high-intensity ultrashort electric pulse. *Phys Rev E Stat Nonlin Soft Matter Phys, 69*(5 Pt 1), 051901. doi:10.1103/PhysRevE.69.051901

Energy-landscape-model analysis for irreversibility and its pulse-width dependence in cells subjected to a high-intensity ultrashort electric pulse

R. P. Joshi,[1] Q. Hu,[1] K. H. Schoenbach,[2] and S. J. Beebe[3]
[1]*Department of Electrical and Computer Engineering, Old Dominion University, Norfolk, Virginia 23529-0246, USA*
[2]*Center for Bio-Electrics, and Department of Electrical and Computer Engineering, Old Dominion University, Norfolk, Virginia 23529-0246, USA*
[3]*Center for Pediatric Research and Department of Physiology, Eastern Virginia Medical School, Norfolk, Virginia 23501, USA*
(Received 6 October 2003; revised manuscript received 15 December 2003; published 4 May 2004)

We provide a simple, but physical analysis for cell irreversibility and apoptosis in response to an ultrashort (nanosecond), high-intensity electric pulse. Our approach is based on an energy landscape model for determining the temporal evolution of the configurational probability function p(q). The primary focus is on obtaining qualitative predictions of a pulse width dependence to apoptotic cell irreversibility that has been observed experimentally. The analysis couples a distributed electrical model for current flow with the Smoluchowski equation to provide self-consistent, time-dependent transmembrane voltages. The model captures the essence of the experimentally observed pulse-width dependence, and provides a possible physical picture that depends only on the electrical trigger. A number of interesting features are predicted.

DOI: 10.1103/PhysRevE.69.051901 PACS number(s): 87.50.Rr, 87.17.Aa, 87.16.Dg

I. INTRODUCTION

The use of very high electric fields ($\sim$100 kV/cm or higher) with pulse durations in the nanosecond range [1–3] has been a very recent development in bioelectrics. Traditionally, most electroporation studies have focused on relatively low external electric fields (less than a kilovolt per centimeter), applied over time periods ranging from several tens of microseconds to milliseconds [4]. A number of important aspects associated with the outer cell membrane such as the field-dependent rupture, the influence of medium conductivity and pH, and possibilities for giant pore formation have been analyzed [5], thus contributing to our current understanding on this subject. From a practical standpoint, traditional electroporation and also shorter electrical pulses could be useful for various applications ranging from cellular electroporation [6–8], production of hybridomas [9,10], the injection of xenomolecules such as hormones, proteins, RNA, DNA, and chromosomes [11–17], the electrofusion of dielectrophoretically aligned cells [18,19], and the nonthermal destruction of micro-organisms [20–22]. In addition, *ex vivo* applications of electroporation have involved the treatment of white blood cells [23] and platelets [24] outside the body. In *ex vivo* studies, electroporation was used to load drugs, and the cells were subsequently reintroduction for therapy. Manipulation of the oxygen binding capability [25] and the electroinsertion of proteins [26] has also been carried out. *In vivo* applications have included the delivery of potent anticancer drugs into solid tumors [27,28].

There appear to be inherent advantages in using short electric pulses, and these include (i) negligible thermal heating, (ii) the ability to develop large electric fields and peak powers, with a lower energy input, (iii) the possibility of selecting the desired time scales through pulse width manipulation, and (iv) the ability to penetrate the outer (plasma) membrane, and create large transmembrane potentials across subcellular organnelles. This can effectively open the way to intracellular electromanipulation, without destroying the outer membrane [29]. The commencement of high-intensity, pulsed electric-field work in recent years, has led to the following important observations. (i) It is possible to maintain the integrity of the outer cell membrane despite the high ($\sim$200 kV/cm electric fields. (ii) Multiple pulses have been observed to do more irreversible damage than single-shot electric shocks. (iii) Irreversible cell damage is seen to occur at the intracellular organelles (e.g., mitochondria), while the outer membranes remain intact [29]. (iv) Calcium is released from the intracellular endoplasmic reticulum in response to external voltage pulses [29,30]. (v) Cell apoptosis has been observed [29,31] for cells subjected to the short electrical pulses. In particular, apoptosis has been seen to be mitochondrial dependent and completely unrelated to plasma membrane electroporation. It may be mentioned here, that in the context of such *in vitro* experiments, apoptosis is defined by the presence of several well-defined markers, such as Annexin-V binding, caspase activation, a decrease in forward light-scattering during flow cytometry, and of cytochrome *c* release into the cytoplasm. (vi) Finally, the observed apoptotic behavior appears to depend on the pulse duration. Thus, for cells subjected to external electric fields *at a constant energy level*, much stronger apoptosis markers were observed only for the longer ($\sim$300 ns) pulses, less at the shorter ($\sim$60 ns) durations, and almost negligible effects for a short 10 ns pulse of the same input energy.

We have recently presented concrete experimental data showing a pulse-width dependence on the cell apoptotic behavior [29]. For example, results of *in vivo* studies showing ultrashort pulse induced caspase activation (an apoptotic marker) through FITC-VAD-fmk fluorescence, are shown in Fig. 1. Pulse durations of 10 and 60 ns were used, with a fixed total energy input of 1.7 J/cc from the external field. The activation was seen to be stronger for the longer 60 ns pulse (despite the lower applied external field), as compared to the 10 ns duration. Similarly, Fig. 2 shows data on caspase

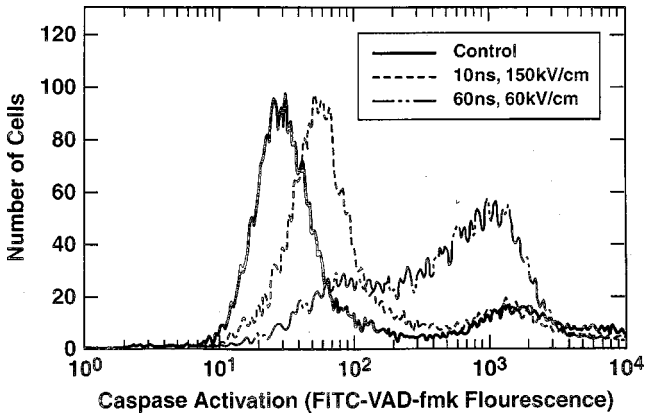

FIG. 1. *In vivo* studies showing ultrashort pulse induced caspase activation (an apoptotic marker) through FITC-VAD-fmk fluorescence. Pulse durations of 10 and 60 ns were used, with a fixed total energy input of 1.7 J/cc from the external field.

activity in Jurkat cells subjected to three pulse durations of 10, 60, and 300 ns, but a fixed total energy of 1.7 J/cc. It might be mentioned that it is experimentally possible to generate fields with a well defined energy output for a given pulse duration as discussed elsewhere [29]. The main result of Fig. 2 is that longer duration pulses are again seen to produce stronger apoptotic behavior, with a clear monotonic trend.

The ability of the short, high-intensity pulses to bring about intracellular damage and apoptotic behavior is not well understood. However, there is now mounting evidence that apoptosis is controlled and regulated by mitochondria in cells [32–36]. This suggests that mitochondria should perhaps be a focal point for the study of cell death and irreversibility brought about by the application of ultrashort electrical pulses. Mitochondria are the cellular power plants assigned to ATP production and maintain a transmembrane proton gradient to drive a variety of tasks [37]. Observations of apoptosis have been indicative of a possible three-step mitochondrial model: (i) an initial phase during which signal

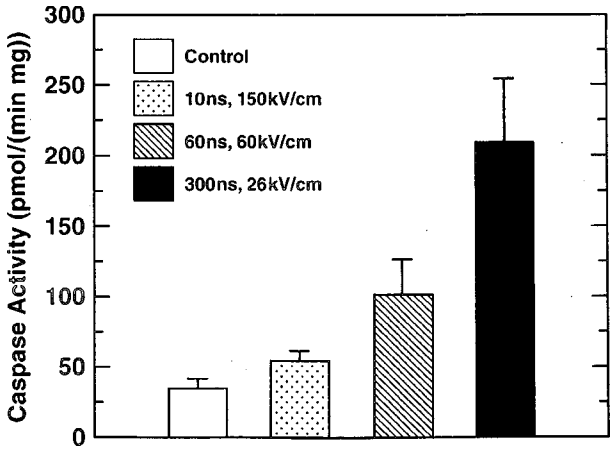

FIG. 2. Data showing caspase activity in Jurkat cells subjected to a single pulse of variable duration, but fixed total energy of 1.7 J/cc. Longer duration pulses are again seen to produce stronger apoptotic response.

transduction cascades or damage pathways are activated, (ii) a mitochondrial phase during which the mitochondrial membrane function is lost, and (iii) a final phase involving protein releases causing the activation of catabolic proteases and nucleases. It has also been established that the release of cytochrome *c* from mitochondria into the cytosol is able to activate procaspases that amplify the cell death process [38]. Cytochrome *c* is a six coordinate, low-spin heme iron species, and is primarily located at the outer face of the inner mitochondrial membrane [39]. This release of cytochrome *c* and other proapoptotic molecules, has been shown [33–36] to be facilitated by a transient opening of the mitochondrial permeability transition pore (MPTP). This mitochondrial permeability transition (MPT) appears to be driven by several factors including calcium overload, oxidative stress, and mitochondrial membrane depolarization. The MPT operates at the crossroads of two distinct physiological pathways, i.e., the Ca^{+2} signaling network during the life of cells, and the effector of apoptotic cascade during Ca^{+2}-dependent cell death [40]. The role of transmembrane potential (along with the pH) on MPT regulation and programmed cell death has now been recognized as well [41]. Since voltage changes are associated with the MPTP that in turn is linked to apoptosis, it is natural to seek a possible link between cell death and transmembrane voltage changes induced by the application of an external voltage pulse.

There is little doubt that action potentials and transmembrane voltages can bring about conformational changes in proteins. Ion channels are common examples in which charge translocation facilitates changes in pore conductivity [42]. More recently, experimental evidence based on Raman spectroscopy has revealed conformational changes in cytochrome *c* at the mitochondrial membranes [43]. The data, which is indicative of the partial opening of the heme pocket and alterations of the heme thioether bonds, provides conclusive evidence of conformational changes in cytochrome *c* [43]. Configurational changes with the proteins of sodium channels, is another example. These changes in conformation can be driven by electrostatic forces associated with nearest neighbor interactions as hypothesized in the "sliding helix" model [44–47]. The voltage controlled, screw-helical mechanism for conductivity modulation has also recently been applied to the study of potassium channels [48,49] and other electrostatic aspects [50,51]. In view of the collective evidence then, we hypothesize that irreversibility and apoptosis in cells subjected to high-field, short duration ($\sim$ nanosecond) pulses may be the result of irreversible conformational changes at the inner mitochondrial membrane driven by the high electric fields arising from strong increases in transmembrane potentials. Qualitative predictions in support of the field dependent irreversibility are presented here on the basis of a simple energy-landscape model.

II. MODELING DETAILS

A. The energy landscape approach

Conformational changes associated with the apoptotic behavior of cells subjected to high-intensity, ultrashort electric pulses could be driven by electrostatic forces arising from

Coulomb interactions between charges (and multipoles) embedded in the proteins and the externally applied electric field. These interactions should give rise to an n-dimensional "energy landscape" whose magnitude is dependent on the position vectors of the constituent charges. Clearly, the details of the various charges at the mitochondrial membrane are very complicated and not fully known. Even if some of the known data were used, an accurate description would not be possible since proteins are capable of movement [52], patterning [53], and self-organization [54], based on a fluid mosaic description of membranes. Hence, a quantitative and precise calculation of the spatial charge distributions and related energy magnitudes is almost intractable. Here, we attempt to present a simple qualitative analysis based on the notion of charge dynamics across an energy landscape in the presence of internal fluctuations and dissipation to account for some of the experimental observations. The central goal is to demonstrate that a simple analysis does capture the central features of the cellular response, and that predictions are in keeping with the observed data. Thus, this model analysis will help provide explanation for the observed effect not being as strong at the shorter 60 ns duration, but being more pronounced for the longer ~300 ns pulse of the same energy.

While the cell membrane system may initially be in equilibrium, the application of an external field changes the landscape and produces charge displacement as the configuration evolves dynamically towards a local energy minima. In this picture, the dynamics of conformational change can then be represented in terms of continuous and random trajectories across the energy landscape defined by electrostatic interactions between the various charges, dipoles, and external electric field in the vicinity of the mitochondrial membrane. In a sense, this amounts to a Markovian model for simulating the time course of electrophysiological events, and is similar to Kramers' theory of activated processes in the condensed phase [55]. Friction must play an important role in the kinetics and the conformational dynamics in response to the applied electric pulses, due to possible energy dissipation into the vibrational modes (confined phonons) of the system. In general, friction always arises due to coupling between the macroscopic mechanical variables (such as the charge displacement) and the various fluctuating, internal degrees of freedom. Frictional losses become especially important for the ultrashort, finite-durations of interest here. This is expected since the final states should depend not only on the initial starting state (possible non-Markovian memory effect), but also on the duration over which the driving force is applied. In addition, there is always a time-lag for the transmembrane potentials to build up (i.e., the membrane charging time), and hence, short-duration pulses can be expected to have a smaller effect than longer pulses. Due to the fluctuating-dissipative nature of the system, the evolution of the mechanical variables can be expected to follow a diffusive Brownian motion across the energy landscape. The concept of using a diffusive motion across an energy landscape was originally proposed by Smoluchowski [56], and subsequently used by Kramers to develop the theory of activated transition rates in the limit of large friction [55]. The Smoluchowski equation for diffusive motion is

$$\partial p/\partial t = \partial[\{p/R(q)\}\{\partial W(q)/\partial q\} + \{k_B T/R(q)\}\,\partial p/\partial q]/\partial q, \tag{1}$$

where p is the probability density of the configurational displacement q at time t. $R(q)$ is the friction coefficient with units of electrical resistance that could be a nonlinear function of the "q" coordinate, while $W(q)$ is the mean potential, k_B the Boltzmann constant, and T the temperature in K. The first term on the right side of Eq. (1) represents drift, while the second denotes diffusion. The diffusion coefficient $D(q)$ is related to the friction coefficient as $D(q)=k_BT/R(q)$. In thermal equilibrium, under steady-state conditions $p(q) \sim \exp[W(q)/(k_BT)]$. Here, a constant frictional coefficient [i.e., $R(q)$ independent of q] will be assumed for simplicity.

Since the energy function $W(q)$ is very complex and is not known for the mitochondria membrane system, we chose to use a harmonic model for simplicity. While this can easily be refined, many of the features observed in pulsed experimental data will nonetheless emerge from this simple model. Besides, the harmonic potential has been applied to voltage gating of the "Shaker" potassium channel [57] based on an energy landscape, and is thus a reasonable starting point. The following form for the energy has been used for ion channels [42,57], with q being assigned units of charge

$$W(q) = aq^2 - qV, \tag{2}$$

where "a" has units of inverse capacitance and taken to equal 3.125×10^{18} F^{-1}, and V is the transmembrane voltage. Here, we assume that conformational change upon the application of an external electric field, is caused by charge movement (with associated displacement "q") in a manner similar to the proposed screw-helical motion within the shaker channel [50]. It is natural and physical to assume then, that charge movement will occur in the presence of other fixed charges within the neighborhood. Consequently, the energy $W(q)$ can be expected to first begin increasing with "q," as the configuration changes from the initial stable state. However, due to the discrete nature of the charge distribution in the vicinity, a local energy minima must exist for larger "q" values. The charges would move into this secondary minima provides the driving force was sufficiently large to slide the chain into the new minimal-energy configuration. In accordance with this model, the energy $W(q)$ has been assumed to have a two-valley, piecewise-parabolic structure shown schematically in Fig. 3. Such a multivalley energy scenario is fairly common in many-body systems, and occurs for example, in the context of conduction electron energies within a crystalline lattice. Figure 3 shows a secondary minima for $q=q_2=1.5q_1$, and a relative barrier at $q=q_1=0.8\times10^{-19}$ C. The overall energy relation $W(q)$ for this model is taken to be

$$W(q) = aq^2 - qV, \quad \text{for} \quad 0 \leqslant q \leqslant q_1 \tag{3a}$$

and

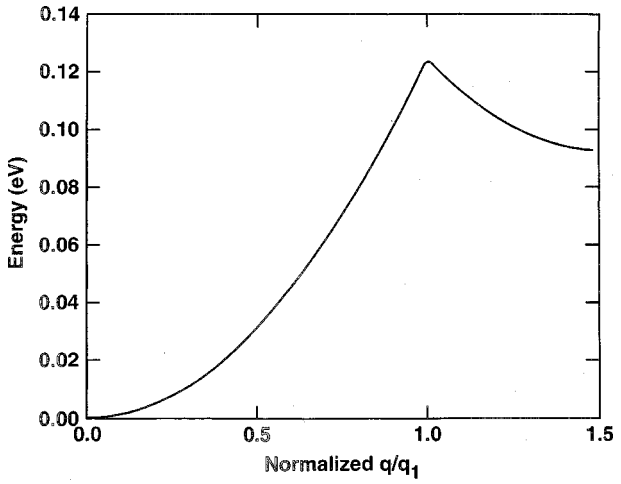

FIG. 3. The simple, two-valley energy landscape model used here for the conformational change calculations. A natural potential barrier at $q=q_1$ and a secondary minima at $q=q_2=1.5q_2$ have been shown.

$$W(q) = a(q-q_2)^2 + aq_2(2q_1 - q_2) - qV \quad \text{for } q_1 \leqslant q \tag{3b}$$

to maintain continuity at $q=q_1$. Such a multivalley, q-dependent model is commonly applied for the analysis of in many physics-related problems of high-field transport. The treatment of charge conduction at high electric fields in semiconductors based on a many-valley, multiband model with bandstructure calculations, is a relevant example [58,59]. The secondary minima in Eq. (3b) has been assigned a higher magnitude than the primary minima at $q=0$. This simply reflects a finite-size effect and the breakdown of translational invariance. For infinitely long strings of translationally invariant discrete charges, the potential would have been periodic. An applied voltage "V" reduces the potential barrier as seen in Fig. 4. The energy function determines drift in configuration space and governs the changes. A positive $E(r)$ slope signifies a driving force towards the initial equilibrium state, while a negative slope forces configurational change. Choosing $q_2=1.5q_1=1.2\times10^{-19}$ C, and $a=3.125\times10^{18}$ the barrier begins to cease at 0.25 V. At 0.375 V a local minima at about $q\sim0.75q_1$ exists, and so a finite configurational change leading to a final stable state is predicted. However, this change would be reversible, since upon removal of the external potential, the energy landscape would revert to the upper $V=0$ curve. Due to a monotonic drift towards the initial equilibrium state, for the $V=0$ situation upon voltage termination, a full recovery to the initial state is predicted. At 0.5 V and higher, the local minima within the central valley, vanishes. This heralds the threshold of a transition into an irreversible regime. For such a case, there is a possibility for continued movement away from equilibrium, even upon voltage termination, provided the system was in a state beyond q_1. Thus, for transient voltage pulses, stability would depend on the ability of the system to drift past the intervalley barrier *maximas within the duration of the applied voltage pulse*. Clearly, very short pulses would not lead to irreversibility. Conversely, a significantly large voltage would be necessary for irreversible destruction for shorter pulse durations. This qualitative reasoning is in keeping with the actual experimental observation, discussed in the next section.

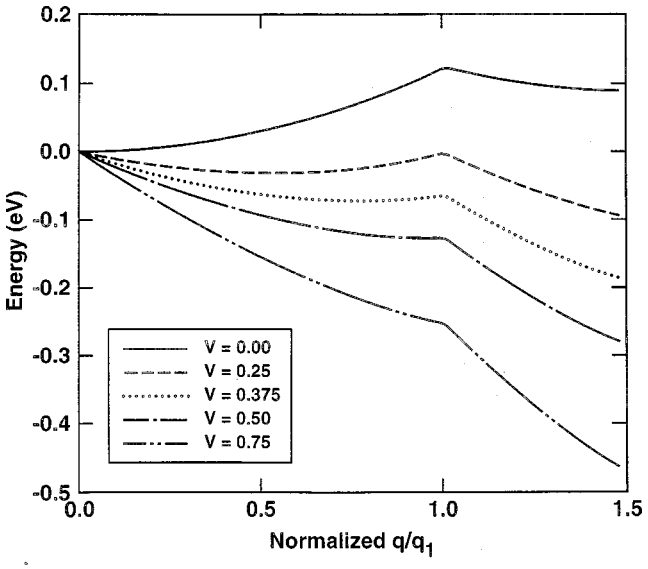

FIG. 4. Effect of various applied voltages on the model energy landscape of Fig. 4.

B. Time dependent electrical calculations

For a more complete and accurate analysis, the temporal evolution of the transmembrane voltage [present in Eqs. (3a) and (3b)], created by the externally applied bias, needs to be determined. An approach to such calculations is through a time-domain nodal analysis involving a distributed equivalent circuit representation of a cell and its membrane structures. Details of this method and its implementation have been given elsewhere [60,61], and so only a brief outline will be discussed here. For simulations, the entire cell volume can be broken up into finite segments, and each segment represented by a parallel RC combination to account for the current flow and charging effects. Using azimuthal symmetry the three-dimensional structure can be mapped into the r and φ coordinates of a spherical system. Here, details of the cell shape were ignored for simplicity. Thus, in the simulations, the computational region was a sphere that included the cell, its substructure, and the surrounding suspension medium. It was discretized along the r and θ direction as shown in Fig. 5. Based on symmetry, only a quarter of the computational region was considered. For simplicity, membranes were taken as an integral unit, i.e., this subregion is not further discretized. For each element, the current continuity equation given below holds:

$$\vec{\nabla}\cdot\left(\vec{J}+\frac{\partial\vec{D}}{\partial t}\right)=0, \tag{4}$$

where J is the current density and D the electric displacement vector. For nodes with index $0<i<n$ and $0<j<m$, as

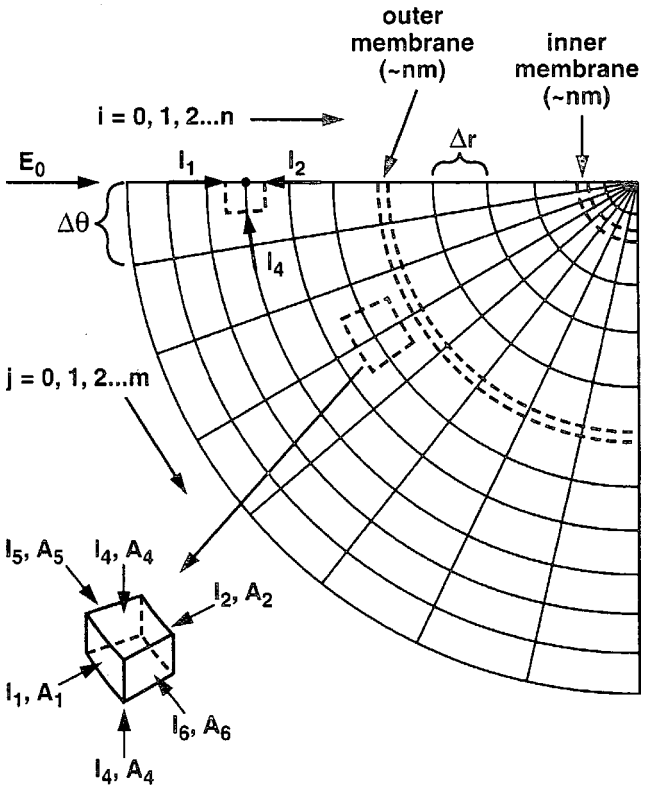

FIG. 5. Schematic of one quarter of the model used to represent a cell for the distributed electrical calculations. The dotted box shows a typical element with current flows.

shown in Fig. 5, the above equation can be rewritten in the following form:

$$\sum_{k=1}^{6}\left(\sigma\vec{E}+\varepsilon\frac{\partial\vec{E}}{\partial t}\right)_k\cdot\vec{A}_k=\sum_{k=1}^{6}I_k=0, \tag{5}$$

where I_5 and I_6 are currents along the ϕ direction, $\vec{A}_k$ is the surface area, $\vec{E}$ the electric field, ε the permittivity, and σ is the conductivity. Considerations of geometric symmetry of the computation region leads to $I_5=I_6=0$ due to the equipotentials. Consequently, one obtains the following equation discretized in space and time:

$$\begin{aligned}&\sigma_1\frac{V^t_{i-1,j}-V^t_{i,j}}{\Delta r}A_1+\sigma_2\frac{V^t_{i+1,j}-V^i_{i,j}}{\Delta r}A_2+\sigma_3\frac{V^t_{i,j-1}-V^t_{i,j}}{r\Delta\theta}A_3\\&+\sigma_4\frac{V^t_{i,j+1}-V^t_{i,j}}{r\Delta\theta}A_4+\frac{\varepsilon_1}{\Delta t}\left[\frac{V^{t+1}_{i-1,j}-V^{t+1}_{i,j}}{\Delta r}-\frac{V^t_{i-1,j}-V^t_{i,j}}{\Delta r}\right]A_1\\&+\frac{\varepsilon_2}{\Delta t}\left[\frac{V^{t+1}_{i+1,j}-V^{t+1}_{i,j}}{\Delta r}-\frac{V^t_{i+1,j}-V^t_{i,j}}{\Delta r}\right]A_2+\frac{\varepsilon_3}{\Delta t}\left[\frac{V^{t+1}_{i,j-1}-V^{t+1}_{i,j}}{r\Delta\theta}\right.\\&\left.-\frac{V^t_{i,j-1}-V^t_{i,j}}{r\Delta\theta}\right]A_3+\frac{\varepsilon_4}{\Delta t}\left[\frac{V^{t+1}_{i,j+1}-V^{t+1}_{i,j}}{r\Delta\theta}-\frac{V^t_{i,j+1}-V^t_{i,j}}{r\Delta\theta}\right]A_4\\&=0.\end{aligned} \tag{6}$$

In the above, $V^t_{i,j}$ stands for the potential at node (i,j) at time t. The radial distance between nodes (i,j) and (n,m) is r. The areas A_1 through A_4 are shown in Fig. 5. Also, σ_1 through σ_4, and ε_1 through ε_4 are the conductivities and permittivities, respectively, at faces 1–4. Thus, if a node were to be within the environment medium, then all the σ values would be the same. However, for nodes on a membrane, σ_1 would be different from σ_2.

In order to reduce the computation load, special boundary conditions were applied, and only a quarter of the entire spherical computational region was considered based on the inherent symmetry. Nodes with $j=0$ and $j=m$ had to be treated carefully. Only I_1, I_2, and I_4 are nonzero since, the targeted element only has 5 faces as face 3 shrinks to a line. For $j=0$ and $0<i<n$, Eq. (6) becomes

$$\begin{aligned}&\sigma_1\frac{V^t_{i-1,j}-V^t_{i,j}}{\Delta r}(r\Delta r/2)^2[\cos\theta-\cos(\theta+\Delta\theta/2)]\\&+\sigma_2\frac{V^t_{i+1,j}-V^t_{i,j}}{\Delta r}(r-\Delta r/2)^2[\cos\theta-\cos(\theta+\Delta\theta/2)]\\&+\sigma_4\frac{V^t_{i,j+1}-V^t_{i,j}}{r\Delta\theta}r\Delta r\sin(\theta+d\theta/2)+\frac{\varepsilon_1}{\Delta t}\left[\frac{V^{t+1}_{i-1,j}-V^{t+1}_{i,j}}{\Delta r}\right.\\&\left.-\frac{V^t_{i-1,j}-V^t_{i,j}}{\Delta r}\right](r+\Delta r)^2[-1-\cos(\theta+\Delta\theta/2)]\\&+\frac{\varepsilon_2}{\Delta t}\left[\frac{V^{t+1}_{i+1,j}-V^{t+1}_{i,j}}{\Delta r}-\frac{V^t_{i+1,j}-V^t_{i,j}}{\Delta r}\right](r-\Delta r/2)^2[-1\\&-\cos(\theta+\Delta\theta/2)]+\frac{\varepsilon_4}{\Delta t}\left[\frac{V^{t+1}_{i,j+1}-V^{t+1}_{i,j}}{r\Delta\theta}-\frac{V^t_{i,j+1}-V^t_{i,j}}{r\Delta\theta}\right]\\&\times r\Delta r\sin(\theta+\Delta\theta/2)=0.\end{aligned} \tag{7}$$

In the above, $\theta=\pi+j\times\Delta\theta=\pi$ and $\Delta\theta$ is $(\pi/2)/m$. For an electric field applied along the z direction (as shown in Fig. 5) and potential at node with $i=n$ is zero, i.e., $V_{n,j}=0$. Nodes with index $j=0$ are equipotentials, so $V_{i,m}=V_{n,j}=0$. Another boundary condition to be considered is for nodes with $i=0$. The potentials of such nodes is calculated as $V_{0,j}=-E_0R\cos\theta$, for $j=0\cdots m$, where E_0 is the externally applied electrical field and R the radius of the computational region.

Combining with the boundary conditions discussed above, one gets N equations for the N unknown node voltages. These N equations can easily be solved through matrix inversion of the form $Ax=B$. Here A is a sparse coefficient matrix. Potential on each node is easily updated at each time step.

In general, the membrane conductances are dynamic and depend on possible electroporation effects. This aspect has been incorporated into our simulations through the use of a Smoluchowski equation driven pore growth and dynamics. Details of the formation energy, pore dynamics and growth have been discussed at length in our previous contributions [60,61]. The development of pores within the membranes (outer cell, mitochondrial membrane, etc.) all depend on the transmembrane voltage, and hence, this is a time- and position-dependent sequence of events. The pore formation and dynamics influences both the conductivity and permittivity (the water-filled pores have an inherently higher dielectric

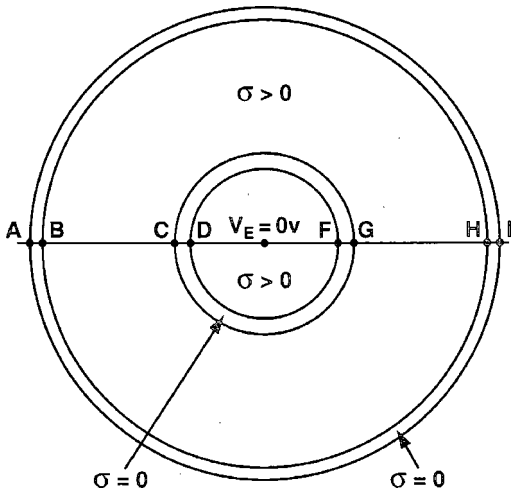

FIG. 6. Sketch of a spherical cell with internal organnelle.

constant than the membranes), and were taken into account for the calculations of total current as given in Eq. (5).

III. RESULTS AND DISCUSSION

Traditionally, electrical pulses with durations on the order of milliseconds and field intensities in the 1–10 kV/cm range have been used [62,63]. Here, however, our focus is on the much shorter nanosecond pulse durations. The advantage of employing such ultrashort pulses is perhaps not immediately obvious, and merits a quick discussion. Figure 6 shows a sketch of a spherical shell with a concentric inner organelle. We assume for simplicity that the conductivities of both membranes are zero, and that current continuity applies across line ABCDE shown in Fig. 6. For long-duration, slow-rising pulses, a near quasisteady state prevails, and the current density J is nearly given by $J=\sigma E+\varepsilon(dE/dr)\sim\sigma E$. Choosing the cell center as the reference voltage, the node potentials are roughly $V_D\sim 0$ and $V_B\sim V_C$. Also, as there is no current flow through the membrane, under quasisteady state $V_{CD}\sim V_{FG}\sim 0$. Thus, the potential across the inner membrane can be expected to be very modest, at best. Fast rising, ultrashort pulses, on the other hand, would force a large nonequilibrium transient, and create substantially large values V_{CD} and V_{FG} across the inner membranes. Thus, ultrashort pulses provide a means for creating *high transmembrane voltages across the subcellular organelles*.

A simple double-shelled cell model was used with the parameters given in Table I that are typical of biological cells, for a quantitative evaluation of the above idea. Most values were chosen from Ermolina [64]. The response of a low intensity 280 ns trapezoidal pulse with $E=5$ kV/cm, and 40 ns rise and fall times, was compared to that of a 11 ns high-intensity trapezoidal pulse with $E=25$ kV/cm, and 1.75 ns rise and fall times. The long pulse bears greater energy. Figure 7 shows the transmembrane potentials across both the inner (nuclear) and outer (plasma) membranes for the longer 280 ns pulse. The inner membrane potential is not seen to rise to large values, and decays down after about 100 ns. This is due to inner membrane discharging and the evolution towards a low inner membrane voltage as qualitatively discussed through Fig. 6. However Fig. 8, for the much shorter 11 ns pulse, shows the inner membrane transmembrane potential could easily reach high magnitudes, well exceeding the outer transmembrane values.

TABLE I. Parameters used in simple simulation.

Conductivities:	
Environment	0.6 S/m
Cell membrane	0.0 S/m
Cytoplasm	0.6 S/m
Organelle membrane	0.0 S/m
Organelle inclusion	0.6 S/m
Relative permittivity	
Environment	80.0
Cell membrane	8.0
Cytoplasm	80.0
Organelle membrane	4.0
Organelle inclusion	80.0
Geometry parameters	
Radius of the simulation region	10 μm
Radius of cell	5 μm
Thickness of cell membrane	5 nm
Radius of organelle	1 μm
Thickness of organelle membrane	10 nm

We now focus on the temporal development of transmembrane voltages and pore radii of mitochondria, based on the distributed, electrical model. In order to model the mitochondria, a concentric triple-shell model as discussed by Asami and Irimajiri [65] was used. The electrical parameters are given in Table II. It may be pointed out that the values of Asami and Irimajiri are not very recent. Hence, it would be useful to generate more refined experimental data for such

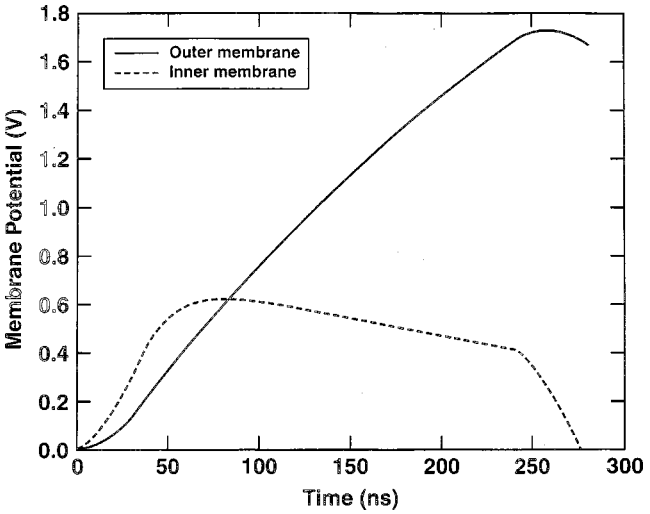

FIG. 7. Transmembrane potential of outer membrane and inner membranes for a 5 kV/cm, 280 ns duration trapezoidal pulse for the cell model of Fig. 4.

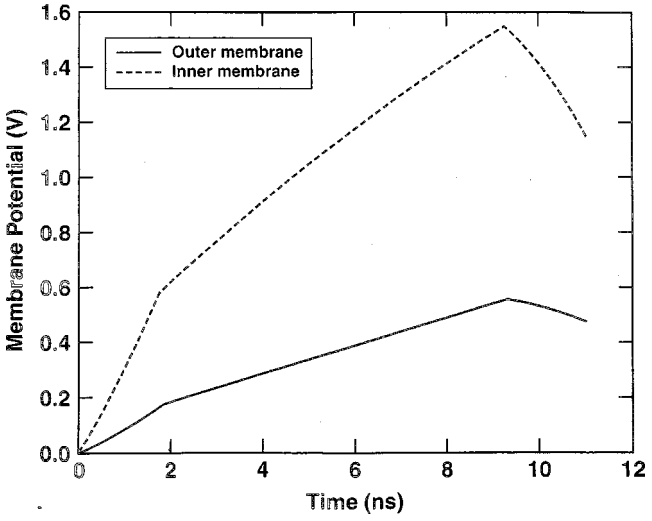

FIG. 8. Transmembrane potential of outer membrane and inner membranes for a shorter 25 kV/cm, 11 ns trapezoidal pulse.

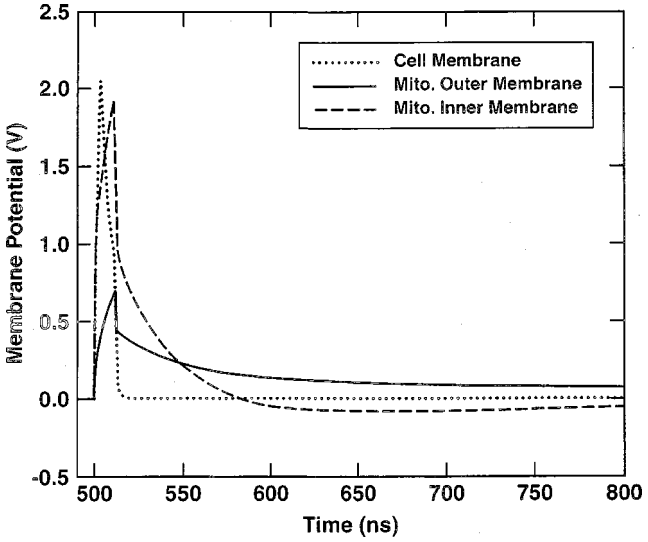

FIG. 9. Time dependent potentials across the outer cell and mitochondrial membranes.

ultrashort, high-field conditions, and carry out a series of simulations to probe the effect of parameter variations. Such efforts are underway. Here, we simply present and discuss the pulse-width dependent qualitative trends (that are physically expected to remain valid) based on a set of published data. Figure 9 shows the simulation results for the membrane potentials with time for a cell subjected to a 100 kV/cm pulse with 1.5 ns rise and fall times, and a 10 ns "ontime." Voltages across the outer cell membrane as well as the inner and outer mitochondrial membranes, are shown. Of these, outer mitochondrial membrane is predicted to have the lowest potential. Another significant point is that both the outer cell and the inner mitochondrial membranes are subjected to fairly large transient voltages, with peak values in excess of 1.9 V. Thus, a transient overshoot of the transmembrane potential is predicted. This transient overshoot aspect agrees very well with a recent experimental report by Meier [66] on giant planar lipid membranes. As is well documented, a transmembrane potential of about 1.0 V is known to cause electroporation under steady-state conditions, or for long-pulse durations. However, as shown by us previously [2], it is possible to exceed the 1 V magnitude during ultrashort transient periods. Physically, since a finite time and energy is required to work against the molecular arrangement within the membrane, excessive voltages over short times seem possible and would not necessarily cause irreversible damage. Also, in Fig. 9, the potential across the outer cell decays much more rapidly, while the transmembrane voltage across the mitochondria is predicted to remain for a much longer time. The initial drop in the outer membrane potential in the simulation arises from electroporation. The pore formation process, whose dynamics and details have been discussed elsewhere [2,60,61], increase the membrane conductivity, leading to the voltage decrease. Effects of changing the time duration of the external voltage pulse for a fixed input energy (i.e., the pulse-width effect) are next examined. Figure 10 shows the time-dependent transmembrane potentials across the inner-mitochondrial membrane obtained from the numerical simulation for 10, 60, and 300 ns pulse widths. In order to keep the overall input energy constant, the electric fields were chosen to have values of 150, 61.23, and 27.38 kV/cm respectively, for the three durations. This choice of electric fields is based on the actual values used in experimental studies by our group [29]. In Fig. 10, the highest membrane voltage is at about 1.8 V, and occurs for the shortest 10 ns pulse. With increasing pulse duration, the peak voltages decrease in keeping with the role of membrane capacitive time constants on the temporal development. The following aspects are evident from the curves of Fig. 10. (i) First, the peak transmembrane voltages do not scale with the externally applied electric field. This is in part due to the voltage-modulated conductivity changes at the membranes. Hence, despite very high external electric fields, it would not necessarily be possible to create as large a voltage across the

TABLE II. Parameters of mitochondria in the triple-shell model [65].

Conductivities (S/m)	
Cell membrane	0.0
Cytoplasm	0.95
Mitochondria membrane	0.95×10^{-6}
Outer compartment of mito.	0.4
Inner compartment of mito.	0.121
Relative permittivity	
Cell membrane	8.0
Cytoplasm	87.7
Compartment of mitochondria	54
Outer membrane of mito.	12.1
Inner membrane of mito.	3.4
Geometry parameters	
Diameter of mitochondria	0.92 μm
Thickness of mitochondria membranes	7 nm
Thickness of outer compartment	30 nm

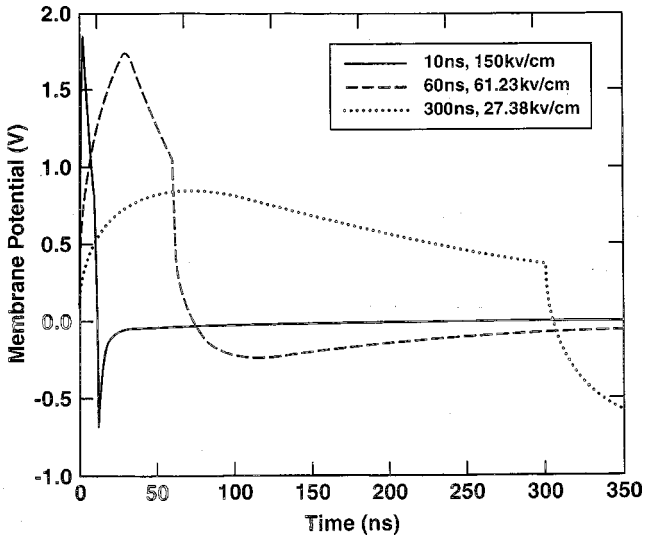

FIG. 10. Time dependent transmembrane potentials across the mitochondrial membranes for 10, 60, and 300 ns pulses.

membranes. (ii) In all cases, the transmembrane voltage begins to decay soon after the external pulse is turned off. The fastest fall off is for the highest external field. (iii) Despite the gradual reduction in transmembrane potential for the 300 ns pulse, its value remains relatively high throughout the entire duration. Thus, a larger electrical energy is available within the biosystem for the 300 ns pulse.

Finally, the energy landscape model was applied to probe the dynamical behavior in response to an externally applied ultrashort, high-intensity electric pulse. The specific aim was to ascertain whether irreversibility (and hence, apoptosis) might have a pulse width dependence at fixed input energy, as seen experimentally. To this end, time-dependent membrane voltages obtained in Fig. 10 were used as inputs to construct the dynamical energy surface from the Smoluchowski equation (1). A numerical solution of Eq. (1) provided the temporal evolution of the probability function $p(q,t)$. Since the friction coefficient $R(q)$ is not well known, a value of $2\times10^3\Omega$ which is in the experimental range reported by Sigg [57], was chosen for these calculations. Results obtained from our simulations, in response to the 10, 60, and 300 ns pulses are shown in Fig. 11. The figure shows snapshots of the probability function $p(q)$ at the specific instants of 30, 200, and 600 ns. These times were chosen as they are well beyond the respective pulse durations. Figure 11(a) shows $p(q)$ for the entire q space, while the higher q range corresponding to the secondary valley is given in Fig. 11(b). Occupancy of the region $q/q_1>1$ signifies irreversibility since the intervalley barrier has a magnitude larger than the thermal energy. The equilibrium distribution has a Maxwellian form, while all other $p(q)$ curves are shifted (i.e., have a drifted-Maxwellian shape) due to the energy landscape alteration by the applied voltage. Of these, for the 10 ns pulse, the deviation is the smallest, and hence, nearly all cells are predicted to recover after the applied pulse. The excursion into the secondary valley is minimal. However, for the 60 and 300 ns pulses, a much larger probability of secondary valley occupancy is predicted. Figure 11(b) shows the

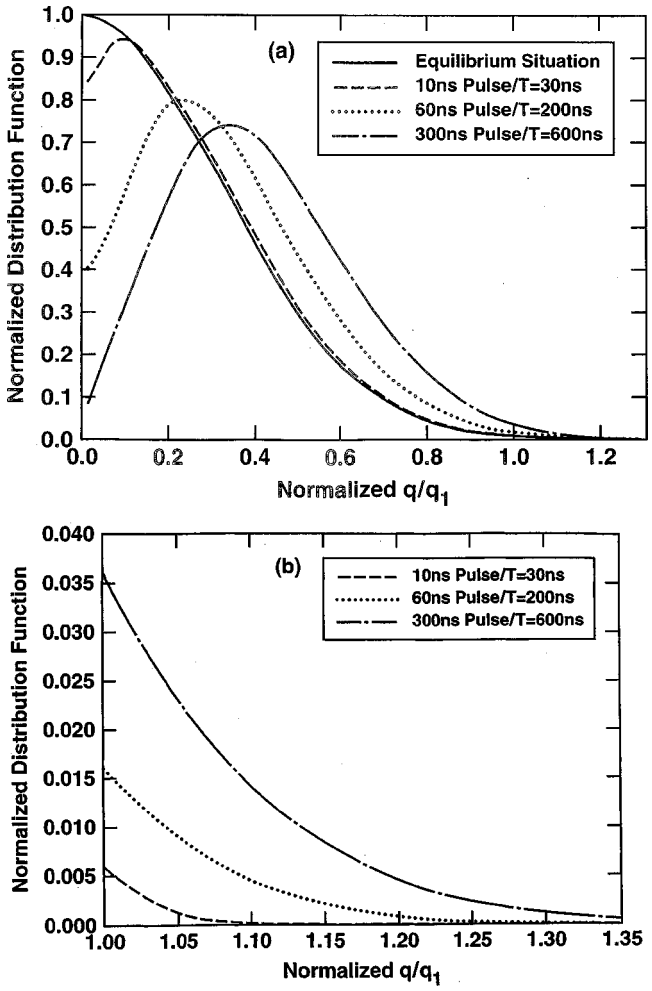

FIG. 11. Simulation results of the occupancy distribution in q space. (a) Snapshots of the equilibrium function and at various times following 10, 60, and 300 ns pulses. (b) Plots emphasizing higher q values within the secondary valley.

probability distribution for $q/q_1>1$, and is clearly indicative of the monotonic increases with pulse duration. A quick calculation of the areal ratios under the three curves of Fig. 11(b) yielded normalized magnitudes of 1.0, 0.333, 0.05 respectively, for the 300, 60, and 10 ns pulses. Thus, almost negligible effects (in terms of irreversibility and possible apoptosis) are predicted from the shortest 10 ns pulse. This is in keeping with experimental results. Also, the trend with the 60 and 300 ns excitation also agree favorably with the progressively stronger marker data for apoptosis and the observed cell mortality numbers.

IV. SUMMARY AND CONCLUSIONS

We have attempted to provide a simple, but physical model for cell irreversibility and apoptosis in response to an ultrashort (nanosecond), high-intensity electric pulse. In view of this collective evidence on cell death and its link to an electrical stimulation, we hypothesize that apoptotic behavior may be the result of irreversible conformational changes at the inner-mitochondrial membrane. Such changes

are likely to be driven by the high electric fields that arise from strong transient increases in transmembrane potentials. Our approach is based on an energy landscape model, which is used to determine the temporal evolution of the configurational probability distribution function $p(q)$. Such an energy landscape picture is not new, and has been used in the description of protein changes [67], as well as the folding and unfolding of small globular proteins [68]. In fact, configurational diffusion as a model for protein relaxation was first suggested by Agmon and Hopfield [67].

The primary emphasis here is on qualitative predictions of an observed pulse width dependence on cell irreversibility. A comprehensive and accurate treatment of this problem is extremely difficult and challenging given that apoptosis can have several pathways, the sequential details of the biophysics are not well known, and neither are the magnitudes of the internal energies and configurations. Given the various difficulties, the present model merely attempts to provide a possible physical picture that is dependent only on the electrical trigger, and captures the experimentally observed pulse-width dependence.

Our model is probabilistic through the use of the Smoluchowski equation and it couples a distributed electrical model for current flow to provide the time-dependent transmembrane voltages. The results agree the observed experimental data very well. Based on the present model, we predict a number of interesting features. (i) First, cell irreversibility at a fixed input energy will depend on the pulse width, and is likely to have an optimal range. Pulses that are very short would not have a significant effect due to insufficient durations for electric field driven conformational changes. On the other hand, much slower and longer pulses would also be rendered ineffective due to their inability to penetrate the membranes of the inner organnelles and develop a significant transmembrane voltage. (ii) The electrical effects are likely to be cumulative and to exhibit a memory effect, provided successive pulses were to be applied with delay times less than that required for complete recovery of the $p(q)$ profiles. Such a memory effect has indeed been noted in the context of the ultrashort, high-intensity pulsing. (iii) The inherent probabilistic basis of this model, implies that complete and total killing of cell populations can never be achieved by a single shot exposure. There will always be a finite probability distribution below the threshold because of the diffusive motion in energy space. Only at very low temperatures might one expect cohesive and "ballistic" motion. This prediction of incomplete killing is in keeping with experimental observations. (iv) Furthermore, this model predicts that the use of very high electric field intensities may not necessarily have a significantly larger impact. This naturally follows since not only is the pulse duration an important factor, but also because the transmembrane potential would not scale with the applied field. Electroporation and dynamic changes in conductivity would work to offset the impact of larger external fields. (v) Here the irreversibility mechanism is taken to arise from fixed charge and dipole movements brought about within the membrane by the electrostatic driving force produced by the large transient transmembrane potentials. Consequently, excitation processes that cannot generate large electric fields at membranes, or if their time durations are small, might not be very effective in electrically triggering apoptotic behavior in cells. For example, under "contactless" conditions, or for microwave and radio-frequency excitation, cellular apoptosis may be expected to be fairly negligible. Such a trend has indeed been observed in some recent studies involving cells subjected to pulsed microwave radiation [69].

Finally, we emphasize that here we have attempted to obtain qualitative trends on the pulse-width dependence based on a simple energy landscape picture. In theory, more refined estimates and quantitative predictions might be possible by incorporating a better energy description of the membrane system. A first step might be the use of randomly-correlated energy models, as first proposed by Derrida [70]. Refinements to include correlation effects, is an interesting possibility as has been shown recently in the context of heteropolymers [71].

ACKNOWLEDGMENTS

This work was sponsored in part by the Air Force Office of Scientific Research (Grant No. F49620-01-1-0506) on Bio-Inspired Concepts and an AFOSR-MURI grant (Grant No. F49620-02-1-0320) on Subcellular Responses to Narrowband and Wideband Radio Frequency Radiation. The authors would also like to acknowledge useful discussions with Professor J. Weaver (MIT) and Professor E. Neumann (University of Bielefeld).

[1] K. H. Schoenbach, S. J. Beebe, and E. S. Buescher, Bioelectromagnetics (N.Y.) **22**, 440 (2001).
[2] R. P. Joshi, Q. Hu, R. Aly, K. H. Schoenbach, and H. P. Hjalmarson, Phys. Rev. E **64**, 11913 (2001).
[3] K. H. Schoenbach, F. E. Peterkin, R. W. Alden, and S. J. Beebe IEEE Trans. Plasma Sci. **25**, 284 (1997).
[4] H. Huelsheger, J. Potel, and E. G. Niemann, Radiat. Environ. Biophys. **20**, 53 (1981).
[5] For example, C. Wilhelm, M. Winterhalter, U. Zimmermann, and R. Benz, Biophys. J. **64**, 121 (1993); R. Benz, *ibid.* **54**, 25 (1988).
[6] U. Zimmermann and G. A. Neil, *Electromanipulation of Cells* (CRC, Boca Raton, FL, 1996).
[7] U. Zimmermann, G. Pilwat, and F. Riemann, Z. Naturforsch. C **29**, 304 (1974).
[8] J. C. Weaver, IEEE Trans. Plasma Sci. **28**, 24 (2000).
[9] M. M. Lo, T. Y. Tsong, M. K. Conrad, S. M. Strittmatter, L. D. Hester, and S. H. Snyder, Nature (London) **310**, 792 (1984).
[10] U. Karsten, P. Stolley, I. Walther, G. Papsdorf, S. Weber, K. Conrad, L. Pasternak, and J. Kopp, Hybridoma **7**, 627 (1988).
[11] A. K. Banga and M. R. Prausnitz, Trends Biotechnol. **16**, 408 (1998).

[12] E. Eksioglu-Demiralp, S. Kitada, D. Carson, J. Garland, A. Andreef, and J. C. Reed, J. Immunol. Methods **275**, 41 (2003).
[13] M. F. Kalady, M. W. Onaitis, K. M. Padilla, S. Emani, D. S. Tyler, and S. K. Pruitt, Surg. Forum **52**, 225 (2001).
[14] G. Mellitzer, M. Hallonet, L. Chen, and S. L. Ang, Mech. Dev. **118**, 57 (2002).
[15] L. Zhang, L. Li, G. Hoffmann, and R. Hoffmann, Biochem. Biophys. Res. Commun. **220**, 633 (1996).
[16] R. L. Harrison, B. J. Byrne, and L. Tung, FEBS Lett. **435**, 1 (1998).
[17] R. Langer, Nature (London) **392**, S5 (1998).
[18] H. Mekid and L. M. Mir, Biochim. Biophys. Acta **1524**, 118 (2001).
[19] C. Ramos and J. Teissie, Biochimie **82**, 511 (2000).
[20] K. H. Schoenbach, R. P. Joshi, R. H. Stark, F. C. Dobbs, and S. J. Beebe, IEEE Trans. Dielectr. Electr. Insul. **7**, 637 (2000).
[21] A. J. H. Sale and W. A. Hamilton, Biochim. Biophys. Acta **148**, 781 (1967).
[22] A. J. H. Sale and W. A. Hamilton, Biochim. Biophys. Acta **163**, 37 (1968).
[23] S. Sixou and J. Teissie, Biochim. Biophys. Acta **1028**, 154 (1990).
[24] K. Hughes and N. Crawford, Biochim. Biophys. Acta **981**, 277 (1989).
[25] U. Broggemann, E. C. Roux, J. Hanning, and C. Nicolau, Transfusion (Bethesda, Md.) **35**, 478 (1995).
[26] M. Zeira, P. Tosi, Y. Mouneimne, J. Lazarte, L. Sneed, D. J. Volsky, and C. Nicolau, Proc. Natl. Acad. Sci. U.S.A. **88**, 4409 (1991).
[27] L. M. Mir, S. Orlowski, J. Belehradek, and C. Paoletti, Eur. J. Cancer **27**, 68 (1991).
[28] M. Okino and H. Mohri, Eur. J. Cancer **27**, 68 (1991).
[29] S. J. Beebe, P. M. Fox, L. J. Rec, L. K. Willis, and K. H. Schoenbach, FASEB J. **17**, 1493 (2003).
[30] J. Deng, K. H. Schoenbach, E. S. Buescher, P. S. Hair, P. M. Fox, and S. J. Beebe, Biophys. J. **84**, 2709 (2003).
[31] S. J. Beebe, P. M. Fox, L. J. Rec, K. Somers, R. H. Stark, and K. H. Schoenbach, IEEE Trans. Plasma Sci. **30**, 286 (2002).
[32] S. A. Susin, N. Zamzami, and G. Kroemer, Biochim. Biophys. Acta **1366**, 151 (1998).
[33] A. P. Halestrap and C. Brenner, Curr. Med. Chem. **10**, 1507 (2003).
[34] A. P. Halestrap, G. P. McStay, and S. J. Clarke, Biochimie **84**, 153 (2002).
[35] M. Crompton, Biochem. J. **341**, 233 (1999).
[36] G. Kroemer and J. C. Reed, Nat. Med. **6**, 513 (2000).
[37] V. P. Skulatchev, *Membrane Bioenergetics* (Springer-Verlag, Berlin, 1988).
[38] V. Petronilli, D. Penzo, L. Scorrano, P. Bernardi, and F. Di Lisa, J. Biol. Chem. **276**, 12030 (2001).
[39] D. Tyler, *The Mitochondrion in Health and Disease* (VCH Publishers, New York, 1992).
[40] F. Ichas and J. P. Mazat, Biochim. Biophys. Acta **1366**, 33 (1998).
[41] L. Scorrano, V. Petronilli, and P. Bernardi, J. Biol. Chem. **272**, 12295 (1997).
[42] D. Sigg, H. Qian, and F. Bezanilla, Biophys. J. **76**, 782 (1999).
[43] S. Berezhna, H. Wohlrab, and P. M. Champion, Biochemistry **42**, 6149 (2003).
[44] C. C. Chancey and S. A. George, Phys. Rev. E **53**, 5137 (1996).
[45] B. F. Ball and J. A. Rice, Math. Biosci. **112**, 189 (1992).
[46] W. A. Catterall, Science **242**, 50 (1988).
[47] H. R. Guy and P. Seetharamulu, Proc. Natl. Acad. Sci. U.S.A. **83**, 508 (1986).
[48] D. A. Doyle, J. Morais, R. A. Pfuetzner, A. Kuo, J. M. Gulbis, S. L. Cohen, B. T. Chait, and R. MacKinnon, Science **280**, 69 (1998).
[49] E. Perozo, D. M. Cortes, and L. G. Cuello, Science **285**, 73 (1999).
[50] R. D. Keynes and F. Elinder, Proc. R. Soc. London, Ser. B **266**, 843 (1999).
[51] R. D. Keynes and F. Elinder, Proc. R. Soc. London, Ser. B **265**, 263 (1998).
[52] S. J. Singer and G. L. Nicholson, Science **175**, 720 (1972).
[53] P. Fromherz and W. Zimmermann, Phys. Rev. E **51**, R1659 (1995).
[54] M. Leonetti and E. Dubois-Violette, Physica A **257**, 77 (1998).
[55] H. A. Kramers, Physica (Amsterdam) **7**, 284 (1940).
[56] M. Smoluchowski, Phys. Z. **17**, 557 (1916); also, S. Chandrasekhar, Rev. Mod. Phys. **15**, 1 (1943).
[57] D. Sigg, F. Bezanilla, and E. Stefani, Proc. Natl. Acad. Sci. U.S.A. **100**, 7611 (2003).
[58] S. Wigger, M. Saraniti, S. M. Goodnick, and A. Leitenstorfer, J. Comput. Electr. **1**, 475 (2002).
[59] H. E. Nilsson, U. Englund, M. Hjelm, E. Bellotti, and K. Brennan, J. Appl. Phys. **93**, 3398 (2003).
[60] R. P. Joshi, Q. Hu, and K. H. Schoenbach (unpublished).
[61] R. P. Joshi, Q. Hu, K. H. Schoenbach, and H. P. Hjalmarson, Phys. Rev. E **65**, 041920 (2002).
[62] L. V. Chernomordik, S. I. Sukharev, S. V. Popov, V. F. Pastushenko, A. V. Sokirko, I. G. Abidor, and Y. A. Chizmadzhev, Biochim. Biophys. Acta **902**, 360 (1987).
[63] J. Olofsson, K. Nolkrantz, F. Ryttsen, B. A. Lambie, S. G. Weber, and O. Orwar, Curr. Opin. Biotechnol. **14**, 29 (2003).
[64] I. Ermolina, Y. Polevaya, Y. Feldman, B. Ginzburg, and M. Schlesinger, IEEE Trans. Dielectr. Electr. Insul. **8**, 253 (2001).
[65] K. Asami and A. Irimajiri, Biochim. Biophys. Acta **778**, 570 (1984).
[66] W. Meier, A. Graff, A. Diederich, and M. Winterhalter, Phys. Chem. Chem. Phys. **2**, 4559 (2000).
[67] N. Agmon and J. J. Hopfield, J. Chem. Phys. **79**, 2042 (1983).
[68] N. D. Socci, J. N. Onuchic, and P. G. Wolynes, J. Chem. Phys. **104**, 5860 (1996); P. G. Wolynes, J. N. Onuchic, and D. Thirumalai, Science **267**, 1619 (1995).
[69] R. Gilgenbach (private communication).
[70] B. Derrida, Phys. Rev. B **24**, 2613 (1981).
[71] S. S. Plotkin, J. Wang, and P. G. Wolynes, Phys. Rev. E **53**, 6271 (1996).